Electronic and Magnetic Properties of Ni Nanoparticles Embedded in Various Organic Semiconductor Matrices

Björn Bräuer,*,† Yana Vaynzof,‡ Wei Zhao,‡ Antoine Kahn,‡ Wen Li,† Dietrich R. T. Zahn,† César de Julián Fernández,§ Claudio Sangregorio,§ and Georgeta Salvan†

Physics Department, Chemnitz University of Technology, 09107 Chemnitz, Germany, Department of Electrical Engineering, Princeton University, Princeton, New Jersey 08544, and Department of Chemistry, University of Florence and INSTM, 50019, Florence, Italy

Received: November 5, 2008; Revised Manuscript Received: January 24, 2009

Ni nanoparticles with a size distribution from 2 to 6 nm, embedded in various organic matrices, were fabricated in ultrahigh vacuum. For this purpose metal free and Ni phthalocyanine, fullerene C_{60}, and pentacene were coevaporated with Ni. When coevaporated, Ni and H_2Pc react, leading to the formation of NiPc and Ni nanoparticles. The molecular structure of the matrix was found to have negligible effect on the size of the nanoparticles but to influence the magnetic anisotropy of the nanoparticles: Ni nanoparticles formed in the buckyball matrix have a cubic symmetry, while nanoparticles formed in matrices consisting of planar molecules exhibit a uniaxial symmetry. After exposure to atmosphere, photoelectron spectroscopy investigations demonstrate the presence of metallic Ni nanoparticles accompanied by Ni oxide and the existence of a charge transfer from the organic matrix to the particles in all investigated systems. The oxidized Ni nanoparticles exhibit a larger magnetic anisotropy compared to the freshly prepared particles which show superparamagnetic properties above 17 K. Moreover, photoelectron spectroscopy was used to probe the oxidation process of the Ni nanoparticles in different organic matrices. It could thus be shown that a matrix consisting of spherical molecules like C_{60} prevent the particles much better from oxidation compared to matrices of flat molecules.

Introduction

Nanosized particles of ferromagnetic metals such as Fe, Co, and Ni are the object of growing interest because of a range of interesting physical properties and potential applications such as catalysts, high density magnetic recording media, ferrofluids, and medical diagnostics.[1−5] Recently, an enhancement of quantum efficiency of organic light emitting devices by doping with magnetic nanoparticles was reported.[6] In this context, the energy level alignment and the presence of interface dipoles and/or charge transfer at the interface between the matrix and the particles is an important issue. With decreasing size down to several nanometers, the particles behave like single magnetic domains,[7] leading to a superparamagnetic state for temperatures above the blocking temperature.[8] In addition to size, the chemical and structural properties of the interface between the particles and the surrounding medium play an important role in determining their magnetic properties.[5,9]

Most of the reported studies on magnetic nanoparticles dealt with metal or oxide nanoparticles dispersed in other metal or nonmagnetic oxide materials. Recently, attention was paid to the use of carbon-based molecules as alternative material for matrices. These molecules can exhibit a wide range of properties, be it optical, fluorescence, catalytic, mechanical, or transport properties, that can be combined to the magnetic properties in such a way to obtain novel multifunctional materials.[10] These materials can be particularly interesting for the development of "molecular" spintronic devices. The benefit in using organic molecules for matrices stems from the fact that they have small spin-orbit and hyperfine interactions and thus the electron-spin polarization can be preserved on longer distances as compared to the inorganic semiconductor matrices.[11−13] Such effects have been investigated in heterojunctions,[11,14] granular films,[15−17] and more complex structures.[18a−d] As in the case of inorganic matrices, the chemical interactions between the nanoparticles and the organic surrounding are essentially determining the transport and magnetic properties.

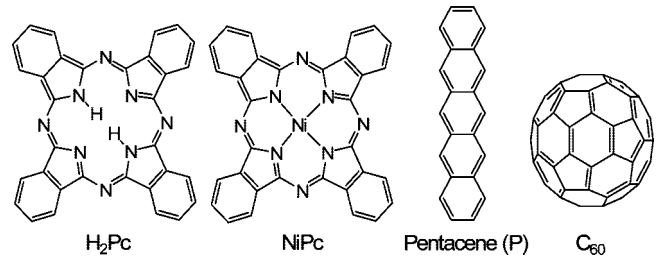

Figure 1. Molecules codeposited with Ni in this work.

A recent approach to fabricate magnetic nanoparticles with size below 25 nm is based on the coevaporation of an organic molecule, fullerene (C_{60}), and the metal in vacuum.[19a] It was suggested that the buckyball C_{60} molecules limit the grain growth and reduce the magnetic coupling between the magnetic particles. It is therefore of great interest to extend the investigations on the formation of metal particles in organic matrices using coevaporation by considering molecules which contain other atomic species besides the carbon atoms, for example, nitrogen and hydrogen atoms.

The present work focuses on the formation of Ni nanoparticles in various matrices consisting of small molecules, outlined in Figure 1. The properties of systems based on phthalocyanine

* To whom correspondence should be addressed. Email: bb@stanford.edu.
† Chemnitz University of Technology.
‡ Princeton University.
§ University of Florence and INSTM.

10.1021/jp809777z CCC: $40.75
Published on Web 03/12/2009

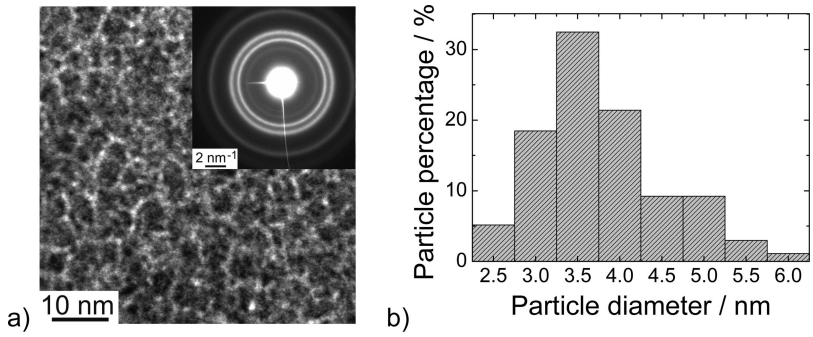

Figure 2. (a) Typical phase-contrast bright-field TEM image recorded for a Ni/H_2Pc film and (b) the statistic size distribution calculated for more than 100 particles. The inset of panel a shows an electron diffraction pattern of the same sample.

matrices, that is, phthalocyanine (H_2Pc) and nickel phthalocyanine (NiPc), are discussed in greater detail, based on the results of structural, Raman spectroscopy, photoelectron spectroscopy, and magnetic investigations. The electronic and magnetic properties of the systems based on the other organic matrices are then comparatively discussed. Special emphasis will be put on studying the ability of various molecular matrices to prevent the Ni nanoparticles from air oxidation.

Experimental Section

The organic source material was thermally evaporated from a Knudsen cell and Ni was evaporated using an electron beam evaporator. The deposition rates were around 2 Å/min for the organic material and 1.5 Å/min for Ni, leading to a ratio of Ni atoms to the number of organic molecules of about 10:1. The films were grown to a nominal thickness of 50 nm onto Si(111) with 2 nm native oxide for the Raman spectroscopy and magnetic susceptibility studies. Photoelectron spectroscopy (PES) investigations were performed on 7 nm thick films deposited onto highly doped hydrogen passivated *n*-Si(111). The substrate was pretreated with a 5% HF solution for 2 min. The high resolution transmission electron microscopy (HR-TEM) and electron diffraction investigations of the NiPc + Ni samples were performed using a Philips CM 20 FEG electron microscope.

The Raman spectra presented in this work were recorded in a macro-configuration at room temperature. The 647.1 nm (1.916 eV) line of a Kr^+ laser was used for excitation. Its energy lies in the lower energy tail of the Q-band optical transition of the used phthalocyanines. The scattered light was collected using a Dilor XY 800 spectrometer with a multichannel charge coupled device detector. The spectral resolution was ~4 cm^{-1} as determined from the full-width at half-maximum (fwhm) of the laser line. The magnetic measurements were performed using a Cryogenic S600 superconducting quantum interference device (SQUID) magnetometer. The X-ray photoelectron spectroscopy (XPS) studies were performed using the Al Kα (1486.6 eV) emission line with a total energy resolution of ~0.9 eV.

Ultraviolet photoemission spectroscopy (UPS) studies were performed using the He I (21.22 eV) and He II (40.81 eV) photon lines of a He-discharge lamp. The photoelectrons were counted with a double-pass cylindrical mirror analyzer. The total energy resolution of the measurement was 0.15 eV, as determined from the width of the Fermi edge measured on a clean poly-crystalline Au(111) substrate. The ionization energy of the film is defined as the energy difference between the vacuum level, determined in a standard way from the position of the onset of photoemission spectrum, and the extrapolated leading edge of the highest occupied molecular orbital (HOMO).

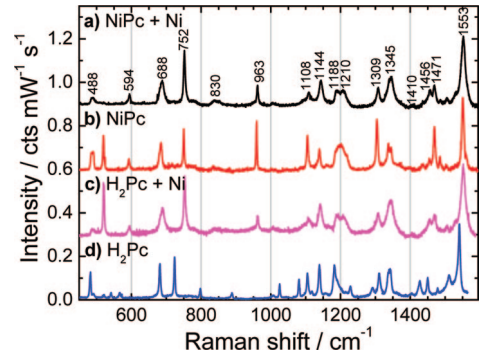

Figure 3. Raman spectra of thin films of (a) NiPc+Ni, (b) NiPc, (c) H_2Pc+Ni, and (d) H_2Pc. The spectra were normalized to the intensity of the band at 1553 cm^{-1}. The band observed at 521.5 cm^{-1} in the spectra b and c stems from the optical phonon mode of the Si substrate.

Results and Discussion

Structural and Electronic Properties. ***a. H_2Pc and NiPc Matrices.*** High resolution transmission electron microscopy (TEM) combined with electron diffraction studies showed the formation of Ni nanoparticles in all investigated matrices. The size distribution is similar within the experimental error for all the systems: the nanoparticle size ranges between 2 and 6 nm and is centered around 3−4 nm. Exemplary, Figure 2 shows the results for the systems obtained by codeposition of Ni and H_2Pc.

Raman spectroscopy was used to identify the chemical composition of the mixed films. It should be noted that the spectrum of the bare phthalocyanine is identical to that of the powder source materials, confirming that the molecular structure is preserved upon thermal deposition. The Raman spectra of the mixed films obtained by codeposition of Ni and H_2Pc (a) and of Ni and NiPc (c) are compared in Figure 3 to the spectra of the bare phthalocyanine films (40 nm) (H_2Pc (d) and NiPc (b)).

Spectra c and d in Figure 3 show many differences in the Raman shift and intensity of the bands, indicating that the molecular structure of the mixed H_2Pc + Ni films and H_2Pc are significantly different. On the other hand, the spectra of NiPc (b), of the NiPc + Ni films (a), and of the H_2Pc + Ni films (c) are almost identical, suggesting a similar chemical composition of the bare NiPc and the two mixed films.

This indicates that during the deposition process a reaction between the H_2Pc molecules and Ni takes place leading to the formation of NiPc molecules and Ni aggregates. The reaction may take place according to the following equation:

$$n\mathrm{Ni} + \mathrm{H_2Pc} \rightarrow \mathrm{NiPc} + 2\mathrm{H} + (n-1)\mathrm{Ni}$$

A similar reaction behavior was observed for Co atoms reacting with monolayers of porphyrin in ultra high vacuum.[19b] The insertion of the Ni atom into the porphyrin is possibly accompanied by an adsorption of H on Ni followed by the formation of H_2 and its desorption. The latter hypothesis could not be proved so far.

Slight differences are also observable between the spectra of NiPc + Ni (a) and NiPc (b). Some bands are enhanced in the spectra of the mixed films, cf. for example, the out-of-plane deformation vibration δ(CH) at 752 cm^{-1}. A general increase in the fwhm of the bands is observed when nanoparticles are embedded in the system. Two prominent examples are the bands stemming from the deformation vibration of δ(CNC) of the isoindole fragment at 688 cm^{-1} and the stretching vibration ν(NiN) at 1309 cm^{-1}. Such an effect can be caused by deformations of the NiPc molecular geometry induced by and/or charge transfer from/to the Ni particles formed in the mixed films. The latter band is also shifted toward higher frequencies in the spectra of the mixed films possibly reflecting a charge transfer from the NiPc to the Ni nanoparticles. A detailed assignment of the Raman bands for NiPc is given in ref 20.

All the investigated samples were exposed to air for 10 days (thus named "aged films") before the PES investigations. From UPS investigations the work function of the Ni(II) ion in NiPc and of the oxidized Ni nanoparticles embedded in NiPc was found to range between 3.8 and 3.9 eV range, cf. Figure 4. These values are slightly below the value of 4.1 eV characteristic for the oxidized Ni and well below the work function of pure Ni, which can vary between 5.0 and 5.4 eV depending on the crystal face.[21]

The Ni 2p XPS spectra of the thin films under investigation are shown in Figure 5a−c. Selected fitting parameters are outlined in Table 1. For comparison the spectrum of a pure 7 nm Ni film is shown in Figure 5b. The decomposition of the Ni 2p core level emission assumes a spin−orbit splitting ($2p_{1/2}$ and $2p_{3/2}$) of 17.5 eV and a statistical branching ratio of 1:2 for p-levels. The Ni $2p_{3/2}$ spectra were fitted in order to determine the ratio of Ni to NiO_x where NiO_x stands for oxygen defective NiO. The bands at 853.4 and 856.8 eV are assigned to Ni and NiO_x, respectively. The band for Ni^{2+} in NiPc is found at 856.4 eV and in the range from 862 to 865 eV a complex multiplet structure occurs. The presence of both the Ni and NiO_x bands indicates that the nanoparticles have a metallic character and are most probably surrounded by an oxide shell. From the total area ratio of the bands assigned to Ni and NiO_x the relative amount of NiO_x was estimated to almost 75% in the mixed NiPc + Ni films. Thus most of the Ni is oxidized within a distance from the surface equal to the information depth of XPS. The TEM images, however, do not show the presence of crystalline NiO_x, indicating that most of the NiO_x must be present in an amorphous state.

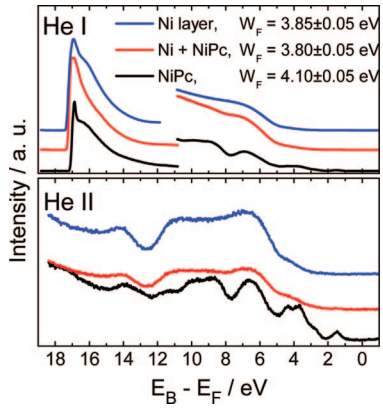

Figure 4. Filled states of three Ni containing layers measured by UPS.

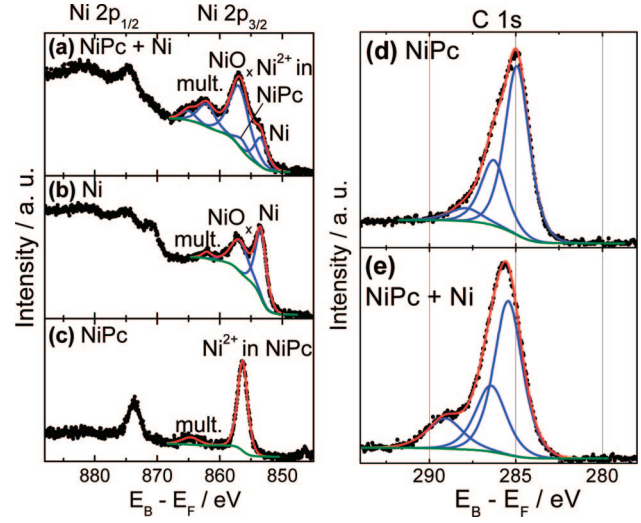

Figure 5. Left panel: XPS spectra of the Ni 2p core levels of (a) codeposited NiPc with Ni, (b) oxidized Ni film, (c) NiPc. Right panel: XPS spectra of the C 1s core levels of (d) NiPc and (e) codeposited NiPc with Ni. All films were exposed to air for 10 days.

TABLE 1: XPS Fit Parameters for the Ni 2p Core Levels Shown in Figures 5 and 6

band	E/eV	rel. area
	(a) NiPc + Ni	
Ni	853.4	1
Ni^{2+} in NiPc	856.4	0.36
NiO_x	856.8	3.27
multiplet	862.0	1.07
multiplet	865.0	0.38
	(b) Ni	
Ni	853.4	1
NiO_x	856.8	0.74
multiplet	862.0	0.08
	(c) NiPc	
Ni^{2+} in NiPc	856.4	
multiplet	864.7	0.14
	(d) C_{60} + Ni	
Ni	853.5	1
NiO_x	857.1	1.25
multiplet	862.2	0.41
	(e) P + Ni	
Ni	853.9	1
NiO_x	856.9	4.29
multiplet	862.3	2.26

The C 1s core level spectra of the thin films under investigation are shown in Figure 5d,e. Selected fitting parameters are summarized in Table 2. Since the spectral resolution is limited to ~0.9 eV, not all components of the C 1s core level can be fitted separately, and several atoms with similar chemical shifts were therefore grouped in the same class. For NiPc, the C 1s peak was resolved into three components with the following binding energies: 284.9 eV for the aromatic carbon of the benzene rings, 286.3 eV for the pyrrole carbon linked to nitrogen, and 287.9 eV for the shakeup satellites of the pyrrole carbon in good agreement with the literature.[22] The codeposition

TABLE 2: XPS Fit parameters for the C 1s Core Levels Shown in Figures 5 and 7

E/eV	rel. area	*E*/eV	rel. area
(a) NiPc		(b) NiPc + Ni	
284.9	1	285.4	1
286.3	0.4	286.5	0.4
287.9	0.1	288.8	0.3
(c) C_{60}		(d) C_{60} + Ni	
285.2	1	285.3	1
287.7	0.2	288.5	0.2
(e) P		(f) P + Ni	
284.5	1	285.4	1
285.4	0.5	286.5	0.2
289.6	0.06	289.0	0.2

of Ni and NiPc induces a shift of the C 1s signal to higher binding energies. The two main carbon peaks are shifted by around 0.3−0.5 eV. The satellite peak cannot be resolved since a new superimposed peak appears at 288.8 eV. Because of its high intensity the new peak is assumed to arise from partial oxidation of a certain amount of NiPc molecules. This behavior can be attributed to a partial charge transfer from the NiPc close to the nanoparticles to the oxidized Ni nanoparticles in agreement with the Raman spectroscopy results.

b. C_{60} and Pentacene Matrices. In Figures 6 and 7, the XPS spectra corresponding to the Ni 2p and C 1s core level of the thin films consisting of Ni particle in C_{60} and pentacene matrices exposed to air for 10 days are shown, respectively. Selected peak fitting parameters are summarized in Tables 1 and 2.

In all cases the presence of metallic Ni is observed, demonstrating that Ni nanoparticles are formed in all organic matrices used. The ratio of NiO_x to Ni peaks seems to be strongly dependent on the molecular structure of the matrix. Compared to the Ni nanoparticles embedded in NiPc the ratio of NiO_x was found to be smaller for C_{60} matrices, cf. Table 1 and 2. For pentacene, the concentration of NiO_x is slightly higher than for the NiPc matrix. The low amount of oxidized Ni in C_{60} should be due to the spherical structure of C_{60} that can enclose the particles more densely than the other molecules studied.

Compared to Ni in NiPc the shift of the C 1s peak for Ni in C_{60} matrix is much less pronounced. This fact can be explained considering that the ionization potential of C_{60} (6.2 eV)[23] is higher than that of NiPc (5.0 eV),[24] which prevents an effective charge transfer from C_{60} to the Ni. However, the C 1s spectra show that not all C_{60} molecules experience the same chemical environment in the mixed films: a part of the C_{60} molecules appears to interact stronger with the Ni nanoparticles leading to an intense peak at 288.5 eV due to a partial charge transfer from C_{60} to the oxidized Ni nanoparticles.

For pentacene the XPS spectrum was fitted using two main peaks and a shakeup satellite peak. Shifts of approximately 1 eV were observed for the main peaks in the mixed compared to the pure pentacene film. In addition, a new peak arises at 289.0 eV in the spectrum of the mixed P + Ni film. The appearance of the new peak around 289 eV might be due to a partial charge transfer from some of the organic molecules to the nanoparticles.

Magnetic Investigations. The magnetic hysteresis loops recorded at 3 K are shown in Figure 8 for three investigated systems after subtracting the diamagnetic contribution of the substrate. The Ni + H_2Pc films behave similarly to the Ni + NiPc samples. Since the particle size is similar in all samples, we would expect to observe the magnetization to saturate at

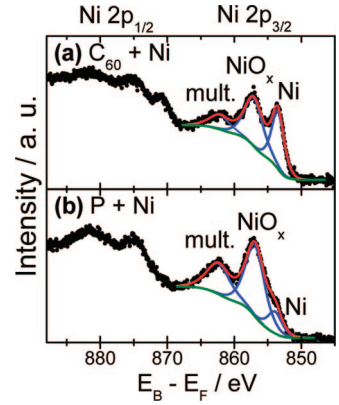

Figure 6. XPS spectra of the Ni 2p core levels of (a) Ni in C_{60} matrix and (b) Ni in pentacene matrix. All films were prepared on *n*-Si substrates and exposed to air for 10 days.

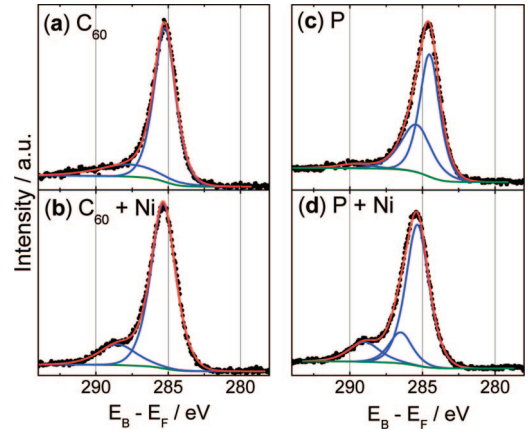

Figure 7. XPS spectra of the C 1s core levels of (a) C_{60}, (b) Ni in C_{60} matrix, (c) P, and (d) Ni in P matrix. All films were prepared on *n*-Si substrates and exposed to air for 10 days.

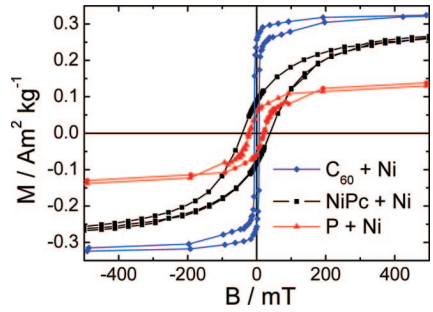

Figure 8. Hysteresis loops of Ni nanoparticles embedded in organic matrices measured at 3 K.

the same value. The observed differences could therefore be related to different percentages of metallic Ni particles in the systems. Indeed, the ratio of Ni to NiO_x was found by XPS to decrease in the same sequence as the magnetic moment in Figure 8 does from C_{60} + Ni, NiPc + Ni, to P + Ni.

Differences were also observed in the temperature dependence of the saturation magnetization of the different samples. Figure 9 displays the temperature dependence of the saturation magnetization (measured in a magnetic field of 5 T), after the subtraction of the diamagnetic contribution of the substrate, normalized to the value measured at a temperature of 3 K. Such a field is already strong enough to saturate the samples within the whole investigated temperature range and the temperature dependence of the magnetization of a superparamagnetic assembly is expected to depend on $T^{3/2}$ (Bloch law). In Figure

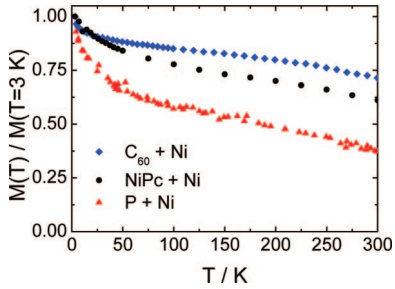

Figure 9. Normalized temperature dependence of the magnetization at an applied field of 5 T of the NiPc + Ni, C_{60} + Ni, and P + Ni samples.

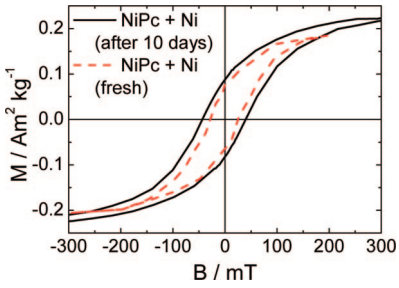

Figure 10. Magnetization versus magnetic field curve measured at 3 K for a sample freshly prepared (dashed line) and after exposure to air for 10 days (continuous line) of NiPc + Ni.

9, the temperature dependence above 75 K is typical for the magnetic behavior of metallic Ni or NiO_x nanoparticles, while below 50 K a significant increase of the magnetization with decreasing temperature is observed. This increase indicates the presence of magnetic species like paramagnetic ions or clusters of NiO_x with frustrated antiferromagnetic order. NiO_x nanoparticles can exhibit a ferromagnetic-like behavior due to the uncompensation of the antiferromagnetic order in the surface atoms or due to the chemical disorder. The magnetic behavior at temperatures near room temperature (RT) is mainly dominated by the contribution from the Ni nanoparticles and the normalized saturation magnetization is larger with the increase of the metal to oxide ratio. In Figure 9, the normalized magnetization at RT decreases in the order C_{60} + Ni > NiPc + Ni > P + Ni, which is in good agreement with the sequence of decreasing amount of Ni to NiO_x ratio, according to the XPS investigations.

Figure 8 also shows that the coercive fields (H_C) of the films differ: the NiPc + Ni has the largest H_C (26 mT), the P + Ni has H_C around 20 mT, while C_{60} + Ni has a coercive field of only 7 mT at a temperature of 3 K. We also found that the remanence to saturation magnetization ratio (M_r/M_s) varies significantly from 0.7 for C_{60} + Ni to 0.4 for P + Ni and down to 0.28 for NiPc + Ni. The size of the Ni nanoparticles is similar in all investigated systems and thus cannot be responsible for the observed variations in H_C and M_r/M_s. As the size of the nanoparticles is in all cases smaller than the critical single domain size of Ni, 50 nm,[25] the magnetization reversal process can be described as a coherent rotation and thus the coercive field is proportional to the magnetic anisotropy and inversely proportional to the saturation magnetization.[7] Thus if all the nanoparticles would have the magnetic anisotropy of the bulk, all investigated systems should show the same H_C, contrary to the experimental observation. In an ensemble of randomly oriented noninteracting nanoparticles M_r/M_s also depends on the nanoparticles size and on the nature of the magnetic anisotropy; the values lie between 0.8 and 0.9 for cubic anisotropy[26] while for uniaxial anisotropy the value is 0.5.[7] The kind of magnetic anisotropy also influences the magnetic barrier and consequently the coercive fields, being larger for uniaxial nanoparticles.[26] Therefore, we propose that the magnetic anisotropy in the C_{60} + Ni is more cubic while in the NiPc + Ni and P + Ni it is more uniaxial.

The different nature of the magnetic anisotropy can originate from different chemical interaction between the surface of the nanoparticles and the surrounding material, both oxide and organic molecules. Moreover, due to the ball-like shape of C_{60} Ni probably grows in a cubic-like crystalline manner; the other molecules are planar and their molecular crystals might induce a uniaxial symmetry of the Ni nanoparticles.

The effect of oxidation on the magnetic properties will be discussed using the example of the NiPc + Ni system by comparing experiments performed on a fresh sample and on a sample exposed to air for 10 days. The hysteresis loops of the fresh and aged films measured at 3 K, cf. Figure 10, show coercive fields of ca. 26 and 40 mT, respectively, while the saturation magnetizations are similar. In the TEM characterizations, we do not observe the presence of core−shell nanostructures with crystalline shells, and neither crystalline phases of the oxide were evidenced. This indicates that the NiO_x present in the systems is amorphous or weakly crystalline, supporting the conclusion drawn above. Amorphous NiO_x, either in form of NiO_x nanoparticles or NiO_x-Ni core−shell structures, can exhibit uncompensation in the antiferromagnetic order and can thus make incoherent rotation processes possible,[28] giving rise to a strong increase of the H_C and of the magnetic anisotropy.

The hysteresis loops of the two samples recorded at 3 K after cooling in a field of 6 T reveal a small displacement of the cycles toward negative fields, cf. Figure 10. This effect can be quantified by the exchange field $\Delta H_C = (H_{C+} - H_{C-})/2$ and is found to be equal to 2 mT for both samples. Such a shift is characteristic for the presence of oxide−metal exchange coupling at the nanoparticles surface.[27−29] The small value of ΔH_C observed here indicates that the coupling between the Ni nanoparticles and the NiO_x present in the system is weak.

The magnetization versus temperature behavior of freshly prepared codeposited NiPc + Ni sample cooled in zero magnetic

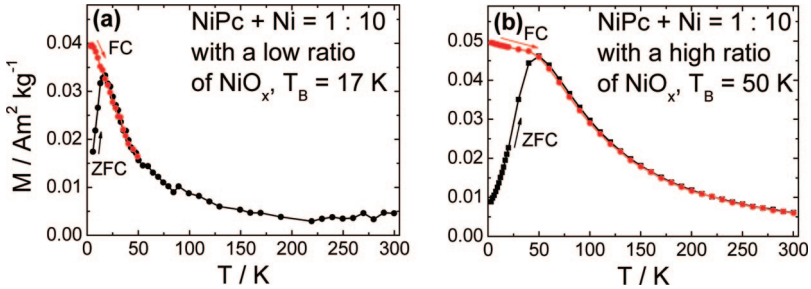

Figure 11. Temperature dependence of the magnetization for a ZFC and FC (5 mT) experiment performed on (a) a freshly prepared sample and (b) an air-exposed sample of NiPc + Ni.

field (ZFC) and in a magnetic field (FC) of 5 mT is shown in Figure 11a. The observed magnetization behavior is typical for particles with a size of just a few nanometers. The ZFC curve exhibits a maximum at a temperature defined as the blocking temperature (T_B = 17 K) above which all nanoparticles are superparamagnetic. At smaller temperatures, thermal irreversibility between the ZFC and FC curves appears, indicating a blocked behavior. The sharpness of the ZFC peak, cf. Figure 11a, reflects a highly monodisperse nature of the Ni nanoparticles[30,25] embedded in NiPc. In Figure 11b, the ZFC and FC magnetization curves for the aged NiPc + Ni film are shown. The magnetic behavior deviates significantly from that of the freshly prepared sample. The blocking temperature shifts to 50 K in the oxidized samples and the ZFC peak becomes broader.

T_B is proportional to the particle volume and to the effective magnetic anisotropy.[8] As the oxidation process is expected to yield in most cases a decrease in the particle volume, the shift of T_B toward higher temperatures and the broadening of the ZFC peak in the aged film must be caused by a strong increase of the magnetic anisotropy which can be produced by the ferromagnetic−antiferromagnetic exchange. Moreover, below T_B a difference in the two FC magnetization curves in Figure 11a,b is observed, which indicates a change in the magnetic properties upon aging in air; while in the fresh sample the magnetization decreases sharply when approaching T_B, in the aged sample the FC magnetization decrease is less pronounced. The latter can be indicative of a spin-glasslike behavior, as often observed in antiferromagnetic metal oxide nanoparticles.[31,32]

From the above discussions we deduce that in both cases the Ni nanoparticles are chemically and magnetically interacting with NiO_x but the NiPc + Ni sample that was exposed to air for 10 days has both H_C and T_B larger than the fresh sample, indicating an increase of the magnetic anisotropy. Such changes can be ascribed to the further oxidation of the metal nanoparticles. However stoichiometric changes, chemical disorder, or structural changes in the NiO_x magnetically coupled to the Ni nanoparticles cannot be ruled out.

Summary

In summary the codeposition of Ni and various molecules is shown to yield the formation of Ni nanoparticles with a controlled size distribution between 2 and 6 nm. Since all investigated molecules have similar size, the molecular structure of the matrix hardly effects the size distribution of the Ni nanoparticles but has a significant influence on their oxidation behavior.

Among the investigated molecules, only H_2Pc was found to react with Ni when codeposited, leading to the formation of NiPc and Ni nanoparticles as shown by Raman spectroscopy and PES. All other molecules experience a charge transfer from or to the Ni nanoparticles, favored by the presence of the Ni oxide shell after exposure to atmosphere.

The formation of Ni oxide upon exposure to atmosphere occurs in all organic matrices but its amount depends strongly on the molecule structure and their packing in the organic matrix, as demonstrated by PES studies. C_{60} was found to prevent the nanoparticles from oxygen most effectively due to its most densely packed structure.

In all systems the Ni nanoparticles were shown to behave superparamagnetically. The molecular nature of the matrix was found to influence the magnetic anisotropy of the nanoparticles; while Ni nanoparticles grown in the buckyball matrix have a cubic symmetry, the nanoparticles formed in matrices consisting of planar molecules exhibit a uniaxial symmetry. The oxidation has a strong influence on their magnetic properties, leading to higher blocking temperatures and coercivity.

This work shows that also planar molecules, similar to the previously used fullerenes, are suitable for fabricating metal nanoparticles by codeposition in vacuum and opens ways to control the electronic and magnetic properties of the nanoparticles by a targeted choice of the molecular structure.

Acknowledgment. B. Bräuer thanks the Fonds der Chemischen Industrie and the Marie Curie program for two Ph.D. fellowships and the German Research Foundation (DFG) for a postdoctoral fellowship. Dr. Steffen Schulze is acknowledged for the HR-TEM and electron diffraction measurements. This work was supported by the National Science Foundation (DMR-0705920) and by the Italian FIRB project RBNE033KMA.

References and Notes

(1) Schultz, L.; Schitzke, K.; Wecker, J. *Appl. Phys. Lett.* **1990**, *56*, 868.
(2) Lu, L.; Sui, M. L.; Lu, K. *Science* **2000**, *287*, 1463.
(3) Ozaki, M. *Mater. Res. Bull.* **1989**, *XIV*, 35.
(4) Gleiter, H. *Nanostruct. Mater.* **1992**, *1*, 1.
(5) Bader, S. *Rev. Mod. Phys.* **2006**, *78*, 1.
(6) Sun, C.-J.; Wu, Y.; Xu, Z.; Hu, B.; Bai, J.; Wang, J.-P.; Shen, J. *Appl. Phys. Lett.* **2007**, *90*, 232110.
(7) Stoner, E. C.; Wohlfarth, E. P. *Philos. Trans. R. Soc. London, Ser. A* **1948**, *240*, 599.
(8) Bean, C. P.; Livingston, L. D. *J. Appl. Phys.* **1959**, *30*, 120S.
(9) Bansmann, J.; Baker, S. H.; Binns, C.; Blackman, J. A.; Bucher, J.-P.; Dorantes-Dávila, J.; Dupuis, V.; Favre, L.; Kechrakos, D.; Kleibert, A.; Meiwes-Broer, K.-H.; Pastor, G. M.; Perez, A.; Toulemonde, O.; Trohidou, K. N.; Tuaillon, J.; Xie, Y. *Surf. Sci. Rep.* **2005**, *56*, 189.
(10) Hueso, L. E.; Bergenti, I.; Riminucci, A.; Zhan, Y. Q.; Dediu, V. *Adv. Mater.* **2008**, *19*, 2639.
(11) Tsukagoshi, K.; Alphenaar, B. W.; Ago, H. *Nature* **1999**, *401*, 572.
(12) Naber, W. J. M.; Faez, S.; van der Wiel, W. G. *J. Phys. D: Appl. Phys.* **2007**, *40*, R205.
(13) Rocha, A. R.; García-Suárez, V. M.; Bailey, S. W.; Lambert, C. J.; Ferrer, J.; Sanvito, S. *Nat. Mater.* **2005**, *4*, 335.
(14) Xiong, Z. H.; Wu, D.; Vardeny, Z. V.; Shi, J. *Nature* **2004**, *427*, 821.
(15) Bernien, M.; Xu, X.; Miguel, J.; Piantek, M.; Eckhold, Ph.; Luo, J.; Kurde, J.; Kuch, W.; Baberschke, K.; Wende, H.; Srivastava, P. *Phys. Rev. B* **2007**, *76*, 214406.
(16) Wu, Y.; Hu, B.; Li, A.-P.; Shen, J. *Phys. Rev. B* **2007**, *75*, 075413.
(17) Kusai, H.; Miwa, S.; Mizuguchi, M.; Shinjo, T.; Suzuki, Y.; Shiraishi, M. *Chem. Phys. Lett.* **2007**, *448*, 106.
(18) (a) Bogani, L.; Wernsdorfer, W. *Nat. Mater.* **2008**, *7*, 179. (b) Bräuer, B.; Weigend, F.; Fittipaldi, M.; Gatteschi, D.; Guerri, A.; Ciattini, S.; Reijerse, E. J.; Salvan, G.; Rüffer, T. *Inorg. Chem.* **2008**, *47*, 6633. (c) Bräuer, B.; Weigend, F.; Totti, F.; Zahn, D. R. T.; Rüffer, T.; Salvan, G. *J. Phys. Chem. B* **2008**, *112*, 5585. (d) Bräuer, B.; Zahn, D. R. T.; Rüffer, T.; Salvan, G. *Chem. Phys. Lett.* **2006**, *432*, 226.
(19) (a) Zheng, L. A.; Lairson, B. M.; Barrera, E. V. *Appl. Phys. Lett.* **2000**, *70*, 3110. (b) Gottfried, J. M.; Flechtner, K.; Kretschmann, A.; Lukasczyk, T.; Steinrück, H.-P. *J. Am. Chem. Soc.* **2006**, *128*, 5644.
(20) Liu, Z.; Zhang, X.; Zhang, Y.; Jiang, J. *Spectrochim. Acta, Part A* **2007**, *67*, 1232.
(21) Holzl, J.; Schulze, F. K. Solid Surface Physics. In *Tracts in Modern Physics*; Springer: New York, **1979**; Vol. 85, p 92.
(22) Petraki, F.; Papaefthimiou, V.; Kennou, S. *Org. Electron.* **2007**, *8*, 522.
(23) Cherkashinin, G.; Krischok, S.; Himmerlich, M.; Ambacher, O.; Schaefer, J. A. *J. Phys.: Condens. Matter* **2006**, *18, 43*, 9841.
(24) Petraki, F.; Papaefthimiou, V.; Kennou, S. *Org. Electron.* **2007**, *8, 5*, 522.
(25) de Julián Fernández, C. *Phys. Rev. B* **2005**, *72*, 054438.
(26) Walker, M. P.; Mayo, P. I.; O'Grady, K.; Charles, S. W.; Chantrell, R. W. *J. Phys.: Condens. Matter* **1993**, *5*, 2779.
(27) Meiklejohn, W. H.; Bean, C. P. *Phys. Rev.* **1956**, *102*, 1413.
(28) Nogués, J.; Sort, J.; Langlais, V.; Skumryev, V.; Suriñach, S.; Muñoz, J. S.; Baró, M. D. *Phys. Rep.* **2005**, *422*, 65.
(29) Spasova, M.; Wiedwald, U.; Farle, M.; Radetic, T.; Dahmen, U.; Hilgendorff, M.; Giersig, M. *J. Magn. Magn. Mater.* **2004**, *272−276*, 1508.
(30) Sappey, R.; Vincent, E.; Hadacek, N.; Chaput, F.; Boilot, J. P.; Zins, D. *Phys. Rev. B* **1997**, *56*, 14551.
(31) Binder, K.; Young, A. P. *Rev. Mod. Phys.* **1986**, *58*, 801.
(32) Makhlouf, S. A.; Parker, F. T.; Spada, F. E.; Berkowitz, A. E. *J. Appl. Phys.* **1997**, *81*, 5561.

JP809777Z